Two-Photon Absorption in Three-Dimensional Chromophores Based on [2.2]–Paracyclophane

6 AUTHORS, INCLUDING:

Mariacristina Rumi
Wright-Patterson Air Force Base

49 PUBLICATIONS **2,518** CITATIONS

SEE PROFILE

Joseph W. Perry
Georgia Institute of Technology

321 PUBLICATIONS **11,930** CITATIONS

SEE PROFILE

Two-Photon Absorption in Three-Dimensional Chromophores Based on [2.2]-Paracyclophane

Glenn P. Bartholomew,[†] Mariacristina Rumi,[‡,ǁ] Stephanie J. K. Pond,[ǁ]
Joseph W. Perry,*,[‡,ǁ] Sergei Tretiak,*,[§] and Guillermo C. Bazan*,[†]

Contribution from the Center for Polymers and Organic Solids, Department of Chemistry and Biochemistry, University of California—Santa Barbara, Santa Barbara, California 93106; School of Chemistry and Biochemistry, Georgia Institute of Technology, Atlanta, Georgia 30332; Los Alamos National Laboratory, Theoretical Division, Los Alamos, New Mexico 87545; and Department of Chemistry, University of Arizona, Tucson, Arizona 85721

Received September 26, 2003; E-mail: joe.perry@chemistry.gatech.edu; serg@lanl.gov; bazan@chem.ucsb.edu

Abstract: A series of α,ω-bis donor substituted oligophenylenevinylene dimers held together by the [2.2]-paracyclophane core were synthesized to probe how the number of repeat units and through-space delocalization influence two-photon absorption cross sections. Specifically, the paracyclophane molecules are tetra(4,7,12,15)-(4′-dihexylaminostyryl)[2.2]paracyclophane (**3R_D**), tetra(4,7,12,15)-(4″-(4′-dihexylaminostyryl)-styryl)[2.2]paracyclophane (**5R_D**), and tetra(4,7,12,15)-(4‴-(4″-(4′-dihexylaminostyryl)styryl)styryl)[2.2]-paracyclophane (**7R_D**). The compounds bis(1,4)-(4′-dihexylaminostyryl)benzene (**3R**) and bis(1,4)-(4″-(4′-dihexylaminostyryl)styryl)benzene (**5R**) were also synthesized to reveal the properties of the "monomeric" counterparts. The two-photon absorption cross sections were determined by the two-photon induced fluorescence method using both femtosecond and nanosecond pulsed lasers as excitation sources. While there is a red shift in the linear absorption spectra when going from the "monomer" chromophore to the paracyclophane "dimer" (i.e., **3R** → **3R_D**, **5R** → **5R_D**), there is no shift in the two-photon absorption maxima. A theoretical treatment of these trends and the dependence of transition dipole moments on molecular structure rely on calculations that interfaced time-dependent density functional theory (TDDFT) techniques with the collective electronic oscillator (CEO) program. These theoretical and experimental results indicate that intermolecular interactions can strongly affect B_u states but weakly perturb A_g states, due to the small dipole–dipole coupling between A_g states on the chromophores in the dimer.

Introduction

Strategies to create new organic chromophores with large two-photon absorption (TPA) cross sections are under intense investigation due to their potential use in emerging applications. These new technologies include three-dimensional optical data storage,[1,2] photodynamic therapy,[3,4] two-photon optical power limiting,[5-7] and two-photon three-dimensional microfabrication.[2,8-11] Substantial progress has been made toward the

development of structure-TPA cross section relationships.[12-14] Recent research encompassing synthesis, experiment, and theory has revealed the importance of certain basic structural motifs for TPA-active organic materials.[14,15] Specifically, a framework for mobile π-electrons with electron donor/acceptor groups on the terminal sites with or without donors/acceptors in the middle

[†] University of California—Santa Barbara.
[‡] Georgia Institute of Technology.
[§] Los Alamos National Laboratory.
[ǁ] University of Arizona.

(1) Strickler, J. H.; Webb, W. W. *Opt. Commun.* **1991**, *16*, 1780.
(2) Cumpston, B. H.; Ananthavel, S. P.; Barlow, S.; Dyer, D. L.; Ehrlich, J. E.; Erskine, L. L.; Heikal, A. A.; Kuebler, S. M.; Lee, I.-Y. S.; McCord-Maughon, D.; Qin, J.; Röckel, H.; Rumi, M.; Wu, X.-L.; Marder, S. R.; Perry, J. W. *Nature* **1999**, *398*, 51.
(3) Stiel, H.; Teuchner, K.; Paul, A.; Freyer, W.; Leupold, D. *J. Photochem. Photobiol. A* **1994**, *80*, 289.
(4) Bhawalkar, J. D.; Kumar, N. D.; Zhao, C.-F.; Prasad, P. N. *J. Clin. Laser Surg.* **1997**, *15*, 201.
(5) a) Bhawalkar, J. D.; He, G. S.; Prasad, P. N. *Rep. Prog. Phys.* **1996**, *59*, 1041. (b) He, G. S.; Xu, G. C.; Prasad, P. N.; Reinhardt, B. A.; Bhatt, J. C.; Dillard, A. G. *Opt. Lett.* **1995**, *20*, 435.
(6) (a) Ehrlich, J. E.; Wu, X.-L.; Lee, L.-Y.; Hu, Z.-Y.; Röckel, H.; Marder, S. R.; Perry, J. W. *Opt. Lett.* **1997**, *22*, 1843. (b) Ehrlich, J. E.; Wu, X.-L.; Lee, I.-Y. S.; Hu, Z.-Y.; Röckel, H.; Marder, S. R.; Perry, J. W. In *Materials Research Society Symposium Proceedings. Materials for Optical Limiting II*, Vol. 479; Sutherland, R., Patcher, R., Hood, P., Hagan, D., Lewis, K., Perry, J. W., Eds.; MRS: Pittsburgh, PA, 1997; pp 9–15.
(7) Fleitz, P. A.; Brant, M. C.; Sutherland, R. L.; Strohkendl, F. P.; Larson, J. R.; Dalton, L. R. *Proc. SPIE Int. Soc. Opt. Eng.* **1998**, *91*, 3472.
(8) Maruo, S.; Nakamura, O.; Kawata, S. *Opt. Lett.* **1997**, *22*, 132.
(9) (a) Zhou, W. H.; Kuebler, S. M.; Braun, K. L.; Yu, T. Y.; Cammack, J. K.; Ober, C. K.; Perry, J. W.; Marder, S. R. *Science* **2002**, *296*, 1106. (b) Stellacci, F.; Bauer, C. A.; Meyer-Friedrichsen, T.; Wenseleers, W.; Alain, V.; Kuebler, S. M.; Pond, S. J. K.; Zhang, Y. D.; Marder, S. R.; Perry, J. W. *Adv. Mater.* **2002**, *14*, 194.
(10) (a) Sun, H. B.; Tanaka, T.; Takada, K.; Kawata, S. *Appl. Phys. Lett.* **2001**, *79*, 1411. (b) Kawata, S.; Sun, H. B.; Tanaka, T.; Takada, K. *Nature* **2001**, *412*, 697.
(11) (a) Miwa, M.; Juodkazis, S.; Kawakami, T.; Matsuo, S.; Misawa, H. *Appl. Phys. A* **2001**, *73*, 561. (b) Strickler, J. H.; Webb, W. W. *Proc. SPIE Int. Soc. Opt. Eng.* **1990**, *1398*, 107. (c) Wu, E. S.; Strickler, J. H.; Harrell, W. R.; Webb, W. W. *Proc. SPIE Int. Soc. Opt. Eng.* **1992**, *1674*, 776.
(12) (a) Reinhardt, B. A.; Brott, L. L.; Clarson, S. J.; Dillard, A. G.; Bhatt, J. C.; Kannan, R.; Yuan, L.; He, G. S.; Prasad, P. N. *Chem. Mater.* **1998**, *10*, 1863. (b) Belfield, K. D.; Hagan, D. J.; Van Stryland, E. W.; Schafer, K. J.; Negres, R. A. *Org. Lett.* **1999**, *1*, 1575. (c) Belfield, K. D.; Schafer, K. J.; Mourad, W.; Reinhardt, B. A. *J. Org. Chem.* **2000**, *65*, 4475.
(13) Kim, O.-K.; Lee, K.-S.; Woo, H. Y.; Kim, K.-S.; He, G. S.; Swiatkiewicz, J.; Prasad, P. N. *Chem. Mater.* **2000**, *12*, 284.
(14) Albota, M.; Beljonne, D.; Brédas, J.-L.; Ehrlich, J. E.; Fu, J.-Y.; Heikal, A. A.; Hess, S. E.; Kogej, T.; Levin, M. D.; Marder, S. R.; McCord-Maughon, D.; Perry, J. W.; Röckel, H.; Rumi, M.; Subramaniam, G.; Webb, W. W.; Wu, X.-L.; Xu, C. *Science* **1998**, *281*, 1653.

Scheme 1. Molecular Structures of **3R**, **5R**, **3R_D**, **5R_D**, and **7R_D**
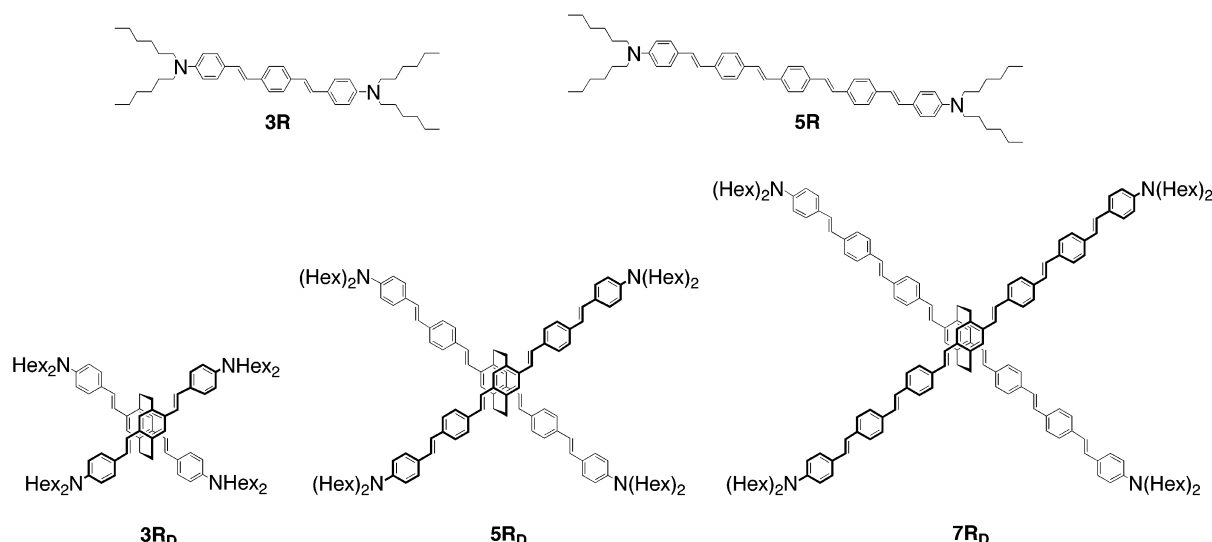
of the conjugated framework provide the potential for symmetric charge displacement upon excitation and enhanced TPA. Much work has focused on linear quadrupolar[14,16] molecules as potential TPA dyes.

More recently efforts have begun on a new area of investigation: the study of the role of three-dimensional, multidirectional charge-transfer chromophores with respect to nonlinear optical (NLO) properties. The "dimensional evolution"[17] of NLO active organic compounds has its roots in the recognition that a higher order charge distribution can give rise to significant quadratic nonlinear responses.[18] This concept has been extended to include the enhancement of cubic nonlinear optical properties within planar octupolar chromophores.[17,19−23] Another strategy toward the enhancement of TPA beyond linear chromophores has been the development of multibranched[24] and/or dendritic chromophores[25−27] where collections of TPA active subunits extend into two or three dimensions.
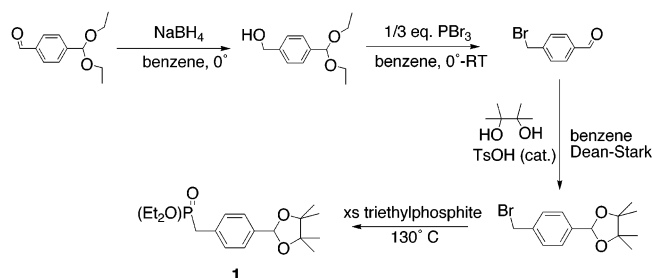
There is unambiguous evidence that the [2.2]paracyclophane (**pCp**) framework can be effectively implemented as a conduit for charge transfer between linear subunits, extending this process from one dimension, within the linear subunit, to three dimensions via "through-space" delocalization.[28] This concept was successfully extended to tetra-substituted **pCp** compounds designed for multidirectional charge transfer within an octupolar template.[29,30] Additionally, **pCp** has been utilized as the locus of interchromophore contacts to systematically study well-defined bichromophoric systems.[31] The structural features and electronic coupling in **pCp**-based chromophores allow for the elaboration of hybrid three-dimensional structures that bring together a "pair" of highly active TPA chromophores with effective through-space interactions.

In this contribution, we present the synthesis, characterization, TPA cross sections, and theoretical description of tetra-donor-substituted **pCp** chromophores with arms of varying length. These molecules have allowed us to examine how a spatial gap across the **pCp** linkage and the distance between electron donor groups across an oligophenylenevinylene segment affect the TPA properties. For reference we also examine the linear counterparts of the **pCp** chromophores. The compounds used for this study are the following: bis(1,4)-(4′-dihexylaminostyryl)benzene (**3R**), tetra(4,7,12,15)-(4′-dihexylaminostyryl)-[2.2]paracyclophane (**3R_D**), bis(1,4)-(4″-(4′-dihexylaminostyryl)-styryl)benzene (**5R**), tetra(4,7,12,15)-(4″-(4′-dihexylaminostyryl)-styryl)[2.2]paracyclophane (**5R_D**), and tetra(4,7,12,15)-(4‴-(4″-(4′-dihexylaminostyryl)styryl)styryl)[2.2]paracyclophane (**7R_D**) (Scheme 1). We report a novel modular synthesis for **5R**, **5R_D**, and **7R_D**. The absorption, emission, and TPA spectra of this series of compounds are examined as a function of conjugated chain length and dimerization of the linear chromophores via the **pCp** linkage. The theoretical modeling of the linear and two-photon absorption spectra and the analysis of the related excited states have been performed using quantum chemical

(15) Rumi, M.; Ehrlich, J. E.; Heikal, A. A.; Perry, J. W.; Barlow, S.; Hu, Z.; McCord-Maughon, D.; Parker, T. C.; Röckel, H.; Thayumanavan, S.; Marder, S. R.; Beljonne, D.; Brédas, J.-L. *J. Am. Chem. Soc.* **2000**, *122*, 9500.
(16) Barzoukas, M.; Blanchard-Desce, M. *J. Chem. Phys. B* **2000**, *113*, 3951.
(17) Hurst, S. K.; Humphrey, M. G.; Isoshima, T.; Wostyn, K.; Asselberghs, I.; Clays, K.; Persoons, A.; Samoc, M.; Luther-Davies, B. *Organometallics* **2002**, *21*, 2024.
(18) (a) Zyss, J. *Nonlinear Opt.* **1991**, *1*, 3. (b) Zyss, J. *J. Chem. Phys.* **1993**, *98*, 6583. (c) Zyss, J.; Ledoux, I. *Chem. Rev.* **1994**, *94*, 77. (d) Joffre, M.; Yarron, D.; Silbey, R.; Zyss, J. *J. Chem. Phys.* **1992**, *97*, 5607. (e) Zyss, J.; Brasselet, S. *Opt. Lett.* **1997**, *22*, 1464. (f) Brasselet, S.; Zyss, J. *J. Opt. Soc. Am. B* **1998**, *15*, 257.
(19) Chérioux, F.; Maillotte, H.; Audebert, P.; Zyss, J. *Chem. Commun.* **1999**, 2083.
(20) Derkowska, B.; Mulatier, J. C.; Fuks, I.; Sahraoui, B.; Phu, X. N.; Andraud, C. *J. Opt. Soc. Am. B* **2001**, *18*, 610.
(21) Cifuentes, M. P.; Powell, C. E.; Humphrey, M. G.; Heath, G. A.; Samoc, M.; Luther-Davies, M. *J. Phys. Chem. A* **2001**, *105*, 9625.
(22) (a) Lee, W.-H.; Lee, H.; Kim, J.-A.; Choi, J.-H.; Cho, M.; Jeon, S.-J.; Cho, B. R. *J. Am. Chem. Soc.* **2001**, *123*, 10658. (b) Cho, B. R.; Son, K. H.; Lee, S. H.; Song, Y.-S.; Lee, Y.-K.; Jeon, S.-J.; Choi, J. H.; Lee, H.; Cho, M. *J. Am. Chem. Soc.* **2001**, *123*, 10039.
(23) Beljonne, D.; Wenseleers, W.; Zojer, E.; Shuai, Z.; Vogel, H.; Pond, S. J. K.; Perry, J. W.; Marder, S. R.; Brédas, J.-L. *Adv. Funct. Mater.* **2002**, *12*, 631.
(24) Chung, S.-J.; Kim, K.-S.; Lin, T.-C.; He, G. S.; Swiatkiewicz, J.; Prasad, P. N. *J. Phys. Chem. B* **1999**, *103*, 10741.
(25) Adronov, A.; Fréchet, J. M. J.; He, G. S.; Kim, K.-S.; Chung, S.-J.; Swiatkiewicz, J.; Prasad, P. N. *Chem. Mater.* **2000**, *12*, 2838.
(26) Varnavski, O.; Leanov, A.; Liu, L.; Takacs, J.; Goodson, T., III. *J. Phys. Chem. B* **2000**, *104*, 179.
(27) Drobizhev, M.; Karotki, A.; Rebane, A.; Spangler, C. W. *Opt. Lett.* **2001**, *26*, 1081.

(28) Zyss, J.; Ledoux, I.; Volkov, S.; Chernyak, V.; Mukamel, S.; Bartholomew, G. P.; Bazan, G. C. *J. Am. Chem. Soc.* **2000**, *122*, 11956.
(29) Bartholomew, G. P.; Bazan, G. C. *J. Am. Chem. Soc.* **2002**, *124*, 5183.
(30) Bartholomew, G. P.; Ledoux, I.; Mukamel, S.; Bazan, G. C.; Zyss, J. *J. Am. Chem. Soc.* **2002**, *124*, 13480.
(31) Bartholomew, G. P.; Bazan, G. C. *Acc. Chem. Res.* **2001**, *34*, 30 and references therein.

Scheme 2. Synthesis of Compound **1**

Figure 1. Absorption and emission spectra of **3R** and **3R_D** in toluene. The emission spectra were obtained by exciting at the corresponding absorption maxima.

calculations with the time-dependent density functional theory (TDDFT) technique.[32,33] This combined study models the behavior of "aggregated" chromophores and examines the impact of through-space delocalization, as well as length-scaling, for TPA active compounds with the goal of providing insight and design guidelines for "three-dimensional" TPA chromophores.

Results and Discussion

Synthesis. Our previous work with tetra-substituted **pCp**-based chromophores led to a synthetic strategy based upon Horner—Emmons coupling to the central **pCp** unit.[29,34] Construction of the donor-terminated oligophenylenevinylene pendants was achieved by a method analogous to the Wittig oxyprenylation,[35] in which a 4-formyl-substituted vinyl group can be added iteratively to the growing conjugated segment. More specifically, we have developed a Horner—Emmons coupling precursor for the stepwise addition of a phenylene-vinylene unit appropriately substituted for continued expansion and/or coupling to the central **pCp** unit.

The required stepwise coupling reagent was synthesized from monoprotected terephthaldehyde and other inexpensive, commercially available starting materials (Scheme 2). Reduction of the unprotected aldehyde with sodium borohydride yields the corresponding benzyl alcohol. This intermediate is easily converted in high yield to the benzylbromide derivative using PBr$_3$ or to the benzyl chloride with thionyl chloride in a slightly lower yield. Reprotection of the remaining formyl group was necessary after halogenation and can be accomplished with either ethylene glycol or pinacol. Finally, conversion to the phosphonate is achieved with the Azburov reaction. The final product, 4,4,5,5-tetramethyl-2-(*para*-methyldiethylphosphonatephenyl)-1,3-dioxolane (**1**), contains a benzylphosphonate functionality for Horner—Emmons coupling and a protected formyl group for additional coupling after a simple deprotection. All steps, with the exception of the one involving thionyl chloride, were of sufficiently high yield and purity that chromatographic separation was not required during workup.

With compound **1**, the arms of the **pCp**-based chromophores can be synthesized iteratively. Coupling of 4-dihexylaminobenzaldehyde to **1** is performed using a small excess (1.2 equiv) of **1** with sodium hydride as the deprotonation agent in THF at 0 °C for 24 h. Following liquid—liquid extraction with methylene chloride and water, the organic layer is filtered through a plug of silica to remove any unreacted **1**. After acid hydrolysis,
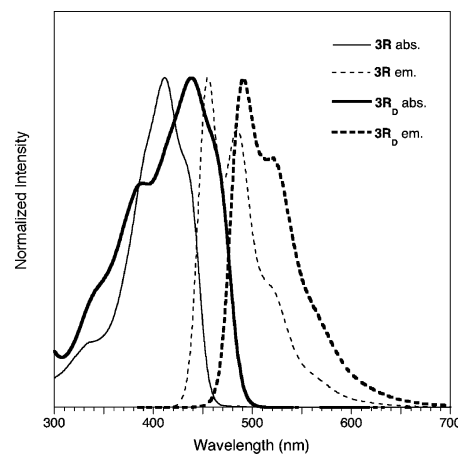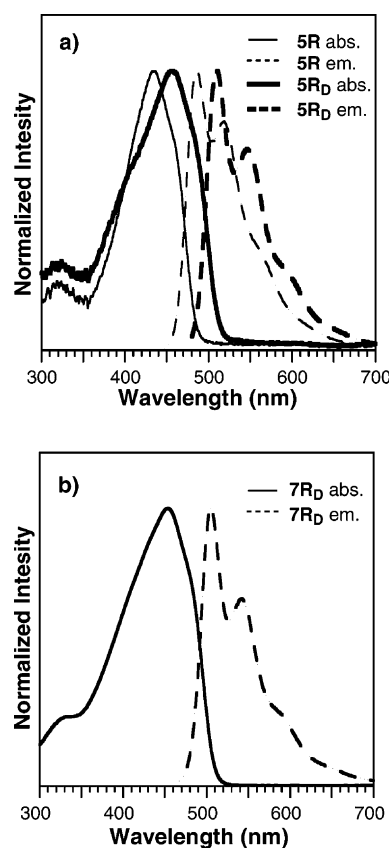
Figure 2. Absorption and emission spectra of (a) **5R**, **5R_D** and (b) **7R_D** in toluene. The emission spectra were obtained by exciting at the corresponding absorption maxima.

the product, 4-dihexylamino-4′-formylstilbene (**2**), is collected in 88% yield. This product can be treated with **1** again in the same procedure to produce 4-dihexylamino-4′-formyldistyryl-benzene (**3**) in 79% yield after purification by chromatography.

Completion of the paracyclophane chromophores was achieved by coupling the appropriate formyl-terminated arm to tetra(4,7,-12,15)-(methyldiethylphosphonate)[2.2] paracyclophane (**4**) using potassium *tert*-butoxide as the deprotonation agent in THF. For example, **4** is reacted with 6 equiv of **2** to yield **5R_D** in 60% yield after trituration of the crude with ethyl ether (Scheme 3). Purity was assessed with ^{1}H NMR spectroscopy and HPLC. Note that this large oligophenylenevinylene dimer was con-

(32) Tretiak, S.; Mukamel, S. *Chem. Rev.* **2002**, *102*, 3171.
(33) Stratmann, R. E.; Scuseria, G. E.; Frisch, M. J. *J. Chem. Phys.* **1998**, *109*, 8218.
(34) Bartholomew, G. P.; Bazan, G. C. *Synthesis* **2002**, 1245.
(35) Spangler, C. W.; McCoy, R. K. *Synth. Commun.* **1988**, *18*, 51.

Scheme 3. Synthesis of Compounds **5R** and **5R_D**
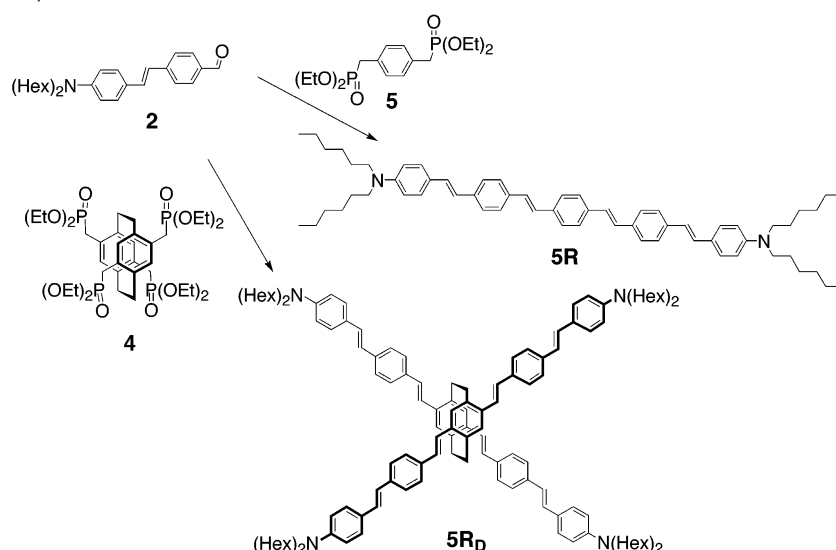
Scheme 4. Synthesis of **7R_D**
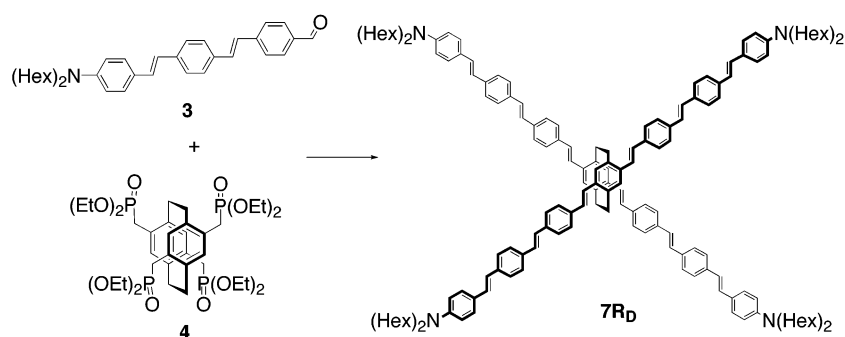
structed from relatively inexpensive starting materials with no preparative chromatography at any step. The linear five-ring compound (**5R**) was synthesized from **2** and α,α′-diethylphosphonate-*para*-xylene (**5**) in 76% yield after column chromatography.

The seven-ring dimer (**7R_D**) was also synthesized in this manner and was purified by preparative HPLC for a final yield of 72% (Scheme 4). It was not possible to generate the linear seven-ring compound (**7R**) under similar conditions to those that led to **5R**. An insoluble red-orange powder formed that could not be completely dissolved in large amounts (200 mg theoretical yield in 1 L) of polar organic solvents such as chloroform and ethyl acetate. Although more extreme dilution throughout workup and purification may have yielded the seven ring linear compound, its solubility would have been too low to perform TPA measurements (concentrations of $\sim 10^{-4}-10^{-5}$ M are usually required) and further purification of this compound was abandoned. Rough solubility estimates of **5R** vs **5R_D** by dilutions in toluene show that **5R_D** is approximately twice as soluble as **5R**. Thus, the more "awkward" geometry of the **pCp**-based compounds yields materials that are more soluble and allows for the examination of **7R_D**, whereas the linear counterpart is not soluble.

Linear Spectroscopy. The absorption and emission spectra of the linear and the corresponding **pCp** dimer compounds were measured in toluene. Figure 1 shows a comparison of spectra for **3R** and **3R_D**. Note the red-shift of the absorption maximum of **3R_D** relative to **3R** (439 nm vs 412 nm, respectively). Also,

a second smaller peak appears in the absorption of **3R_D** at ~ 385 nm. This "Davydov-like" splitting[36] has been observed previously in (4,7,12,15)tetra(4-*tert*-butylstyryl)[2.2]paracyclophane, another dimer in which oligophenylenevinylene segments are joined via their central rings in a "criss-cross" fashion.[37] The emission maximum of **3R_D** is also red-shifted relative to that of **3R** (490 nm vs 453 nm, respectively).

The trends observed in the three-ring compounds are repeated in the five-ring models (Figure 2). The absorption of **5R_D** is red-shifted by 22 nm (0.14 eV) relative to **5R** (457 nm vs 435 nm respectively). The absorption spectrum of **5R_D** also shows a shoulder at ~ 400 nm although it is less pronounced than the splitting in the **3R_D** spectrum. The emission of **5R_D** is also red-shifted relative to **5R** (510 nm vs 485 nm, respectively). Note the red-shift in the absorption of **5R_D** vs **3R_D** of 18 nm (0.11 eV). As expected, increased chain length leads to increased conjugation. The absorption spectrum of **7R_D**, however, reveals a maximum at 454 nm, approximately the same as for **5R_D**. It seems that the saturation value for the energy of the lowest excited state is reached for a chain length of five rings. Recent

(36) The splitting observed in the absorption spectra is qualitatively described by Davydov's familiar model but with one important caveat: theoretical modeling indicates that, beyond excitonic coupling, partial electron exchange occurs between the **pCp** bound "monomers". The absence of formal electron exchange between monomers, however, is part of the construction of the Davydov model. Since no conflicts appear to the authors in the extension of this characterization of the splitting, we note here the difference and from herein refer to the phenomenon as Davydov splitting.
(37) Wang, S.; Bazan, G. C.; Tretiak, S.; Mukamel, S. *J. Am. Chem. Soc.* **2000**, *112*, 1289.

Table 1. Summary of Spectroscopic Data for Linear and **pCp**-Based Chromophores[a]

compd	abs max (nm)	emission max (nm)	Φ_F	ϵ_{max}[b] (M^{-1} cm^{-1})[c]	ϵ_{INT}[c] (M^{-1} cm^{-2})	M_{ge}[d] (D)
3R	412 (405)	453	0.89	8.28×10^4	3.35×10^8	11.3 (13.8)
3R$_D$	439 (434)	490	0.86	1.04×10^5	6.67×10^8	16.4 (20.3)
5R	435 (460)	485	0.92	1.27×10^5	5.40×10^8	14.7 (17.3)
5R$_D$	457 (480)	510	0.87	1.92×10^5	1.02×10^9	20.7 (28.5)
7R	(484)					(21.2)
7R$_D$	454 (495)	506	0.75	2.38×10^5	1.31×10^9	23.3 (32.1)

[a] Data reported are for toluene solutions. Theoretical TDDFT results are given in parentheses. [b] ϵ_{max}: peak extinction coefficient. [c] ϵ_{INT} is defined as the integral of the extinction coefficient over the main absorption band ($\int \epsilon(\omega) \, d\omega$, with ω expressed in wavenumbers). [d] M_{ge} (in Debye, D): transition dipole moment between the ground state (g) and the first excited state (e). See text for the definition of state e in the case of the dimers.

experimental studies suggest longer saturation lengths in oligophenylenevinylenes structurally similar to the molecules in this study.[38] Torsional disorder in the **pCp**-linked molecules may restrict the conjugation to five repeat units, or the influence of the donor substituents on the energy of the lowest one-photon band may be diminished for the longer chain lengths. Studies of the absorption properties of these chromophores as a function of solvent and temperature, as well as studies of related compounds with, for example, different donors, should be conducted to ascertain the origin of this effect.

All of the compounds in this series exhibit a high fluorescence quantum yield in toluene (Φ_F in Table 1). There appears to be a small decrease in Φ_F going from the linear to the dimer models. This decrease is consistent with an increased number of torsional degrees of freedom and is reflected in the value of $\Phi_F = 0.75$ for **7R$_D$**, the largest molecule in the series.

It is interesting to compare the strengths of the electronic transitions that give rise to the absorption bands. The extinction coefficients at the peak of the absorption band (ϵ_{max}) are reported in Table 1. It can be seen immediately that, although ϵ_{max} increases on going from a given linear molecule to the corresponding criss-cross dimer, the magnitude of the increase is different for the three-ring and five-ring systems (ϵ_{max}(**3R$_D$**)/ ϵ_{max}(**3R**) = 1.26 and ϵ_{max}(**5R$_D$**)/ϵ_{max}(**5R**) = 1.51). This is due to differences in the shape of the absorption band among both the linear molecules and the dimers. The relative intensity of the two resultant peaks of the Davydov splitting for the dimers also varies in the series. To take into account the contributions from both components, the extinction coefficients have been integrated over the entire absorption band ($\epsilon_{INT} \equiv \int \epsilon(\omega) \, d\omega$); this quantity is proportional to the oscillator strength of the electronic transition[39]). The results are included in Table 1 and show that ϵ_{INT} approximately doubles on going from the linear to the criss-cross molecules (ϵ_{INT}(**3R$_D$**)/ϵ_{INT}(**3R**) = 1.99 and ϵ_{INT}(**5R$_D$**)/ϵ_{INT}(**5R**) = 1.89). These results suggests that the contributions to the oscillator strength from the two molecules in the criss-cross dimers are additive and that the interaction of the two molecules causes only a redistribution of the overall absorption strength over the two components of the splitting of the electronic band.

For the linear molecules, the absorption band is due to electronic transition between the ground state, g, and the lowest

excited state, e. The corresponding transition dipole moment, M_{ge}, can be evaluated[39] easily and is included in Table 1. A similar approach can be used for the criss-cross molecules if, for the moment, we assume that the overall absorption band is due to a single electronic transition. The values of M_{ge} found in this way appear to increase with chain length. This trend agrees well with previous results for donor-π-donor oligophenylenevinylene derivatives.[15] Specifically, in the molecules studied here, M_{ge} increases approximately with the square root of the total number of double bonds (with each phenyl ring counted as 1.5 double bonds).

TPA Spectroscopy. The TPA cross sections (δ) were determined by the two-photon induced fluorescence method[40] using both femtosecond (fs) and nanosecond (ns) pulsed lasers as excitation sources. The two-photon spectra of the chromophores investigated are displayed in Figure 3 for excitation wavelengths in the range 650−910 nm. It should be noted that the agreement between the femtosecond and nanosecond data, in their overlap region, is very good for molecules **3R** and **3R$_D$** but is less so for the other molecules. However, the data show the same trend in all cases (for example, the δ value is larger at 730 nm than at 750 nm for **5R** and **7R$_D$** according to both the nanosecond and femtosecond results). In addition, it has to be noted that, for an uncertainty of about 15%, *only* in the case of **7R$_D$** the nanosecond and femtosecond data lie outside each other's error bars (but they are within 2 standard deviations of each other). At present, the origin of the discrepancy between the nanosecond and femtosecond data is unknown. However, the conclusions drawn from the data reported in this work are not sensitive to this uncertainty (at most a factor of 1.5). The nanosecond measurements are subject to a larger uncertainty because they were conducted at lower intensities than typically used in our laboratory (by a factor of 4 or 5). This was necessary because, at some excitation wavelengths, deviations from the expected dependence of the signal on the square of the laser intensity were observed at the intensities normally used for other molecules. These deviations indicate the onset of other effects that can occur upon excitation, for example, excited state absorption, photoionization, or other processes that effectively reduce the fluorescence signal or slow the ground-state recovery. For $\lambda \geq 720$ nm, only the data obtained using fluorescein as reference standard have been included in Figure 3 and Table 2. When coumarin 307 was used, values consistently lower (by about 40%) have been obtained. The other spectral characteristics were, however, unchanged.

The spectra of compounds **3R** and **3R$_D$** show only one peak (around 720 nm), while the other compounds clearly show two peaks, one around 720 nm, the other around 810−830 nm. The position of the two-photon peak at the longest wavelength (corresponding to the lowest energy transition and indicated as peak *i* in Table 2) moves to the red with increasing chain length for the linear molecules or the dimers, even if the shift is relatively small going from **5R$_D$** to **7R$_D$**, suggesting that the energy of the two-photon state has reached a saturation value for these compounds. A similar phenomenon is observed in the position of the linear absorption maximum, as described in the previous section.

Overall, the data in Table 2 show that there is an increase in the value of δ for peak *i* (δ_i) with increasing chain length and

(38) Hsu, J. H.; Hayashi, M. T.; Lin, S. H.; Fann, W. S.; Rothberg, L. J.; Perng, G. Y.; Chen, S. A. *J. Phys. Chem. B* **2002**, *106*, 8582.
(39) Herzberg, G. *Molecular Spectra and Molecular Structure. I. Spectra of Diatomic Molecules*, 2nd ed.; Van Nostrand Reinhold Company: New York, 1950.
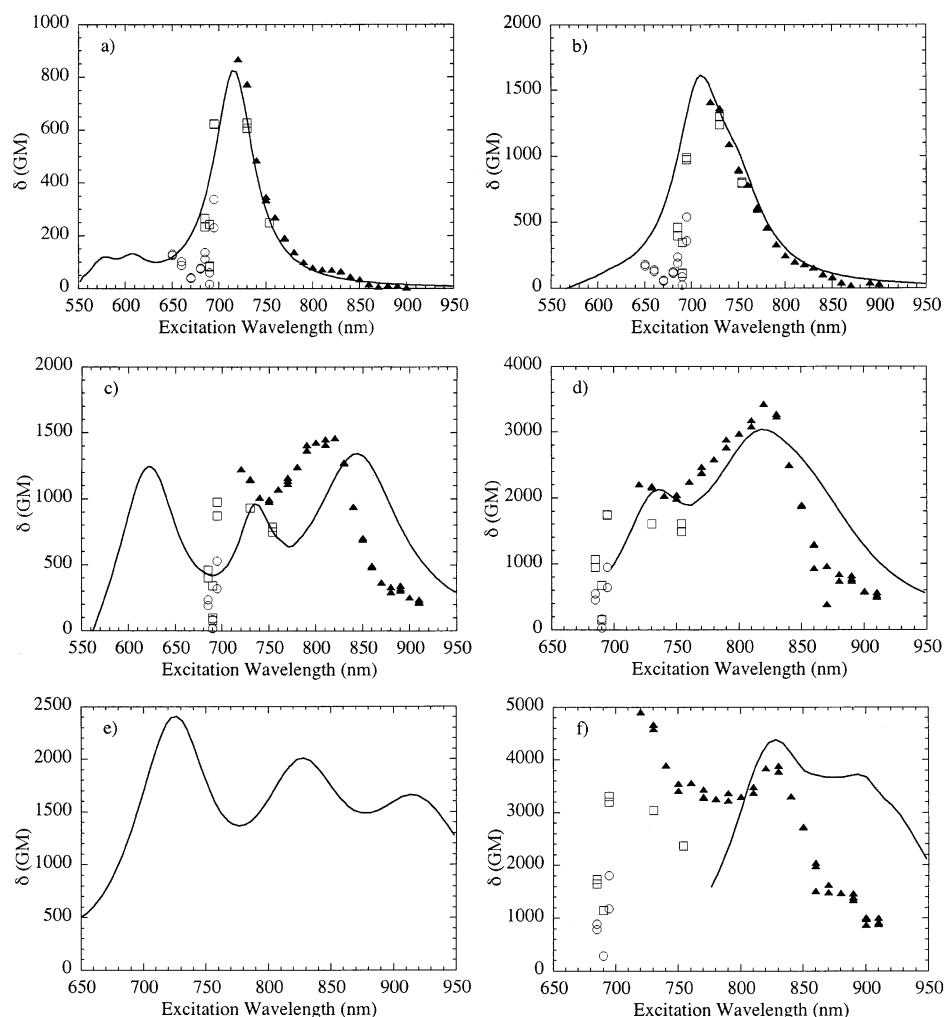(40) Xu, C.; Webb, W. W. *J. Opt. Soc. Am. B* **1996**, *13*, 481.

Figure 3. Experimental and theoretical two-photon induced fluorescence excitation spectra for the following: (a) compound **3R**, (b) compound **3R$_D$**, (c) compound **5R**, (d) compound **5R$_D$**, (e) compound **7R**, and (f) compound **7R$_D$**. Experimental results: (▲) femtosecond measurements using fluorescein as standard; (□) nanosecond measurements using fluorescein as standard; (○) nanosecond measurements using bis(methylstyryl)benzene as standard. Theoretical results: solid line.

Table 2. Two-Photon Absorption Parameters[c] for the Lowest-Energy Peak (*i*) and Highest-Energy Peak (*ii*)

compd	$\lambda_i^{(2)a}$ (nm)	δ_i^b (GM)	$\lambda_{ii}^{(2)a}$ (nm)	δ_{ii}^b (GM)
3R	720 (715)	870 (824)		
3R$_D$	720 (710)	1410 (1615)		
5R	810 (845)	1450 (1345)	720 (735)	1230 (966)
5R$_D$	820 (817)	3430 (3036)	720 (734)	2210 (1938)
7R	(920)	(1652)	(828)	(2013)
7R$_D$	830 (894)	3890 (3730)	720 (828)	4910 (4390)

*$^a \lambda^{(2)}$: position of the peak in the two-photon absorption spectrum. $^b \delta$: peak two-photon absorption cross section (1 GM ≡ 1 × 10^{-50} cm^4 s/photon-molecule); the uncertainty in δ is of the order of 15%. ^{c} Theoretical results are given in parentheses. Line widths $\Gamma = 2 \, (\ln 2)^{0.5}\sigma$ (where σ's are the Gaussian widths from Table 3) have been used to estimate the theoretical magnitudes of the cross sections, except for molecule **7R**, for which a line width of $\Gamma = 0.15$ eV has been used (see text).*

in going from a linear molecule to the corresponding dimer. Moreover, the δ value for peak *ii* (δ_{ii}) increases going from **5R** to **5R$_D$** and to **7R$_D$**. In fact, for **7R$_D$**, peak *ii* is the strongest two-photon peak ($\delta_{ii} > \delta_i$). If the one-photon state is taken to be the intermediate state in a simplified sum-over-states (SOS) description,[14] the large values for δ_{ii} can be explained partly by the smaller energy detuning term (≈1.0 eV) for the two-photon state involved in this transition with respect to the one responsible for peak *i* (1.2−1.3 eV).

When the results for the linear molecules and the corresponding criss-cross dimers are compared, it is immediately apparent that, in contrast to the linear spectra, the shapes of the two-photon spectra are very similar (one peak at the same wavelength in the three-ring case; two bands in approximately the same position in the five-ring case). The peak δ value increases in going from the linear to the criss-cross case, but the ratio is significantly larger in the five-ring case ($\delta_i(\mathbf{3R_D})/\delta_i(\mathbf{3R}) = 1.6$; $\delta_i(\mathbf{5R_D})/\delta_i(\mathbf{5R}) = 2.4$). However, closer inspection of the shape of the spectra indicates that the band of **3R$_D$** is broader than that of **3R**, while the width of peaks *i* in **5R** and **5R$_D$** are similar. This broadening could lead to an effective increase of the ratio reported above for the three-ring case (see below). The broadness of the band in **3R$_D$** could be due to the presence of two unresolved components of the main transition, a result of Davydov splitting due to the coupling between the two chromophores that constitute the dimer, similar to what was observed in the linear absorption spectra. This type of splitting is actually predicted by the quantum chemical calculations, which show it to be small (see Theory section).

We can thus conclude that the two-photon cross section of the criss-cross dimer is approximately twice that of the corresponding linear molecule. An increase of similar magnitude was
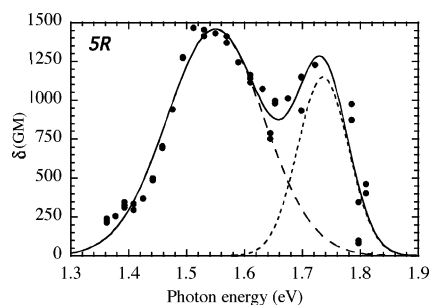
Figure 4. Fitting of the experimental two-photon spectrum of **5R** using two Gaussian bands. (Solid circle) experimental data; (dashed line) best fit to peak *i*; (dotted line) best fit to peak *ii*; (solid line) sum of the two components of the fitting.

Table 3. Fitting Parameters for the Two-Photon Spectra

compd	peak	$\delta_0{}^a$ (GM)	$E_0{}^a$ (eV)	σ^a (eV)	area^b (GM × eV)	$M_{ee'}{}^c$ (D)
3R		805	1.723	0.075	107.0	11.0 (10.1)
3R$_D$		1320	1.704	0.093	217.7	9.5
5R	*i*	1456	1.550	0.119	305.9	15.9 (12.0)
	ii	1149	1.736	0.062	126.3	7.8 (6.5)
5R$_D$	*i*	3261	1.536	0.107	615.9	14.6
	ii	2001	1.729	0.084	299.4	7.6
7R$_D$	*i*	3671	1.543	0.144	939.8	16.2
	ii	4039	1.736	0.075	533.5	9.1

^{a} Each spectrum was fitted using two Gaussian curves of the type: $\delta(E) = \delta_0 \exp[-(E - E_0)^2/\sigma^2]$, where E is the photon energy (expressed in eV), δ_0 is the amplitude of the Gaussian, E_0 is the position of its maximum, σ is the width of the Gaussian (defined as the point at which the value is reduced to 1/e of the maximum), and $\delta(E)$ is the value of δ at energy E. ^{b} Area of each Gaussian curve, defined by $\delta_0 \sigma \pi^{1/2}$. ^{c} Transition dipole moments for the transition between state e and the two-photon state e′ (corresponding to peaks *i* or *ii*) as determined from eq 9 of ref 15. Theoretical results are given in parentheses.

observed for ϵ_{INT}. In an SOS description, this suggests that the values of δ are primarily determined by the transition moment between the ground and the first excited state (M_{ge}) and that there are only small differences in the other transition moments involved.

To better compare the experimental spectra with the results of the quantum chemical calculations, it would be useful to separate the contributions of peak *i* and *ii* (due to the broadness of some of the peaks, the position and the magnitude of the maximum can be affected by the adjacent band). We thus performed a fitting of the experimental spectra using a superposition of two Gaussian band shapes. Although the results are necessarily approximate, they provide some insight into the spectroscopic properties of these chromophores. Gaussians were chosen as fitting curves for their simplicity, even if some of the experimental bands were not symmetric. Even with such approximations, however, the resulting fits are reasonably good for all the molecules, as illustrated in Figure 4 for **5R**. For completeness, a similar fitting procedure, but using only one Gaussian component, was performed on compounds **3R** and **3R$_D$**. Table 3 lists the significant fitting parameters obtained by this method.

It is immediately evident from these results that the widths of the two-photon peaks *i* and *ii* for the same molecule are rather different. Some differences are also observed from molecule to molecule. Consequently, it is more useful to discuss not the amplitudes of the Gaussians (δ_0 or maximum δ values) but their areas, quantities that are related to the integrated two-photon absorption cross section for a given transition and could be

compared more directly with theoretical predictions. Several conclusions can be drawn from the analysis of the band areas (Table 3). First, the area of the two-photon peaks increases by a factor of $\sim$2 going from a linear molecule to the corresponding criss-cross dimer. In particular, area(**3R$_D$**)/area(**3R**) = 2.0, area-(**5R$_D$**,*i*)/area(**5R**,*i*) = 2.0. As suggested above, this indicates that the two-photon absorption cross section for this state is approximately additive in the two components of the dimer. Second, the ratio of the areas for peak *i* and peak *ii* decreases when going from **5R** to **5R$_D$** and to **7R$_D$**: the ratios [area(*i*)/area(*ii*)] are 2.4, 2.1, and 1.8, respectively (note that the trend is not monotonic for the amplitudes of the bands). Third, the area of peak *i* depends approximately linearly on chain length. The increase in the area of peak *ii* with increasing length is instead superlinear.

It is possible to estimate the transition dipole moments between the first excited state (e), and the two-photon state (e′) corresponding to the peaks *i* or *ii*, $M_{ee'}(i)$ or $M_{ee'}(ii)$.[15] The transition moments calculated in this way correspond to orientational averages of the actual molecular transition moments. Table 3 includes the transition moments obtained if the fitting results are used as peak position, amplitude of δ, and width of the peak. It can be seen that the transition moments $M_{ee'}$ are similar for a given linear molecule and the corresponding criss-cross dimer (10−11 D for the three-ring compounds, and 15−16 D for peak *i* for the five-ring ones). This confirms the observation that the molecular parameter most strongly affected by the topology of these chromophores is M_{ge} and not $M_{ee'}$. Moreover, the value of $M_{ee'}(i)$ seems to saturate with the chain length for the longer compound **7R$_D$**. The transitions moments corresponding to peak *ii* are instead smaller than those for peak *i*.

Due to the increased activity and the relative position of the two TPA peaks, the spectra of **5R**, **5R$_D$**, and **7R$_D$** exhibit a broad bandwidth over which the cross section is large. Each of these molecules shows a strong TPA from about 700 to 850 nm, with a cross section over 700 GM for **5R**, over 1000 GM for **5R$_D$**, and over 2500 GM for **7R$_D$**. This $\sim$150 nm bandwidth of the TPA spectra allows for high flexibility in the wavelength used for excitation, which could be a useful feature for applications as two-photon excited fluorescence imaging and optical power limiting. The broad bandwidth may be of use, for example, in multiprobe imaging experiments, in that it gives one a better ability to find a common wavelength for excitation of different TPA dyes that have resolvable fluorescence bands, such that they can be simultaneously excited with a single laser wavelength but can be imaged separately. Additionally, the spectral region of the TPA spectra of these chromophores overlaps very well with the tuning range of Ti:sapphire lasers, which are a preferred source for two-photon fluorescence microscopy.

Theory

Quantum chemical calculations of nonlinear polarizabilities require extensive numerical effort. Time-dependent perturbation theory, which relates the optical response to the properties of the excited states, is typically used to evaluate resonant nonlinear responses, such as δ. For example, the SOS method based on the expansion of the Stark energy of a molecule in powers of the electric field involves the calculations of both the ground state and excited state wave functions and the transition dipole

moments between them.[14] These calculations are usually based on semiempirical model Hamiltonians such as the intermediate neglect of differential overlap/spectroscopy (INDO/S) model, fitted to reproduce UV−visible absorption spectra at the configuration interaction singles (CIS) level, which includes only single-particle electronic correlations.[41] This technique calculates B_u states contributing to the linear optical response of chromophores of the type considered in this article fairly accurately.[37]

However, the situation is very different for A_g states, which contribute to two-photon absorption. Semiempirical techniques accounting solely for single-particle electronic correlations result in a significant blue-shift ($\sim$100−300 nm) for these states compared to the experiment.[42] Accurate calculation of A_g states requires accounting for higher order electronic correlations (such as MRD-CI) which are computationally expensive and typically "ruin" linear absorption states; i.e., the red-shift of A_g states (correct direction) will be typically accompanied by a blue-shift of B_u states (wrong direction), because the ground-state wave function becomes overcorrelated.[14,15]

This problem calls for another more accurate method for computing two-photon states. The TDDFT is a relatively new[33] and increasingly popular approach for computing molecular excited states, which reproduces relatively well both B_u and A_g states,[43] even though the latter have significant double excitation character. In particular, TDDFT has been found to be numerically accurate for the energetics of singlet and triplet A_g states in oligophenylenevinylenes[44] which are structurally similar to the TPA molecules being examined in this paper. The SOS approach cannot be combined with the TDDFT method directly, since the latter does not calculate excited-state wave functions and the transition dipole moments among them. However, the formal similarities of the TDDFT method and the time-dependent Hartree−Fock (TDHF) approach[45] allow one to apply expressions for a nonlinear resonant optical response recently derived for TDHF, to TDDFT as well.[46,47] Alternatively, TPA can be calculated in TDDFT using the single residues of the quadratic response function. This technique has been successfully implemented and tested on several molecules.[48]

We have used a TDDFT approach to calculate the TPA properties as described in refs 46 and 47. The only required input is a set of transition energies and densities describing ground-to-excited state electronic transitions, which is readily available from commercial quantum chemical codes such as the Gaussian 98 program suite.[49] We expect TDDFT to give accurate energies for excited states involved in both one- and two-photon absorption, as demonstrated in the study described in ref 47. However, failure of the conventional exchange−correlation functionals to describe long-range electron transport properties such as charge-transfer excitations[50] may affect the

results for the largest molecules, **7R** and **7R$_D$**. Future studies of the application of TDDFT are necessary to clarify the limitations of this method for the calculation of nonlinear responses in extended molecular systems.

We start our modeling by building the molecular geometries of **3R**, **5R**, and **7R** and their corresponding **pCp**-based dimers (**3R$_D$**, **5R$_D$**, and **7R$_D$**). We use crystal data[51] to derive the structures of the **pCp** core and the oligophenylenevinylene arms. Positions of the remaining atoms, i.e., the hydrogens and the terminal groups (dimethylamino groups were used for the calculations, instead of longer dihexylamino groups), have been optimized using the hybrid B3LYP functional combined with the 6-31G basis set. An extension to larger basis sets usually does not significantly effect the results in large conjugated molecules,[47] since TPA of the molecules in question originates from the response of mobile π-electrons strongly delocalized over the conjugated chains. Thus, the contribution of the atomic polarization is minimal.

The energies and the corresponding transition densities of the singlet excited states were calculated with the TDDFT technique using the Gaussian 98 program suite.[49] Again, the B3LYP/6-31G approach has been used for all calculations described here. The TDDFT method solves the eigenvalue problem (diagonalization of the random phase approximation (RPA) matrix, Λ)

$$\Lambda \xi_\nu = \Omega_\nu \xi_\nu \qquad (1)$$

using the modified Davidson algorithm[52] (as implemented in Gaussian 98).[33] Here, Ω_ν is the transition frequency and ξ_ν is the related transition density given by

$$(\xi_\nu)_{mn} = \langle \nu | c_m^+ c_n | g \rangle \qquad (2)$$

where c_m^+ (c_n) is the creation (annihilation) operator of an electron in the m-th (n-th) atomic orbital, and $|g\rangle$ ($|\nu\rangle$) is the ground (excited) state many-electron wave function. The TDDFT method is numerically much more expensive compared to semiempirical approaches. This limited the calculations to 30 electronic states for each molecule, except for the **7R$_D$** chromophore where the 20 lowest electronic states were calculated. However, these lowest excited states include all the essential states contributing to the linear and two-photon responses of these molecules. For small molecules, we found that the subsequent increase of the number of states has a negligible effect on the UV−visible linear absorption spectrum and changes the magnitude of the related two-photon response by less than 10%, which is mostly attributed to the finite line width of the spectra (see below).

Finally, the linear and two-photon absorption spectra have been calculated using the formalism for optical responses in the time-dependent approaches developed in ref 46. Gaussian 98 (which calculates TDDFT excited states) was interfaced with the collective electronic oscillator (CEO) program[32] (which was modified to use the TDDFT data for calculating optical responses). This is possible, since both the CEO and the TDDFT share the same RPA approximation for the electronic structure.[45] For example, the linear absorption at frequency ω

(41) Ridley, J.; Zerner, M. C. *Theor. Chim. Acta* **1973**, *32*, 111.
(42) Soos, Z. G.; Ramasesha, S.; Galvao, D. S. *Phys. Rev. Lett.* **1993**, *71*, 1609.
(43) Hsu, C. P.; Hirata, S.; Head-Gordon, M. *J. Phys. Chem. A* **2001**, *105*, 451.
(44) Campbell, I. H.; Smith, D. L.; Tretiak, S.; Martin, R. L.; Neef, C. J.; Ferraris, J. P. *Phys. Rev. B* **2002**, *65*, 085210.
(45) Chernyak, V.; Mukamel, S. *J. Chem. Phys.* **2000**, *112*, 3572.
(46) Tretiak, S.; Chernyak, V. *J. Chem. Phys.* **2003**, *119*, 8809.
(47) Masunov, A.; Tretiak, S. *J. Phys. Chem. B* **2004**, *108*, 899.
(48) Salek, P.; Vahtras, O.; Guo, J. D.; Luo, Y.; Helgaker, T.; Ågren, H. *Chem. Phys. Lett.* **2003**, *374*, 446.
(49) Frisch M. J.; et al. *Gaussian 98*, rev. A11; Gaussian, Inc.: Pittsburgh, PA, 2002.
(50) (a) Tozer, D. J.; Amos, R. D.; Handy, N. C.; Roos, B. O.; Serrano-Andres, L. *Mol. Phys.* **1999**, *97*, 859. (b) Neiss, C.; Saalfrank, P.; Parac, M.; Grimme, S. *J. Phys. Chem. A* **2003**, *107*, 140.

(51) Oldham, W. J, Jr.; Miao, Y.-J.; Lachicotte, R. J.; Bazan, G. C. *J. Am. Chem. Soc.* **1998**, *120*, 419.
(52) Davidson, E. R. *J. Comput. Phys.* **1975**, *17*, 87.

is given by the imaginary part of

$$\alpha(\omega) = \sum_\nu \frac{f_\nu}{\Omega_\nu^2 - (\omega + i\Gamma)^2} \qquad (3)$$

where Γ is the line width, and f_ν is the oscillator strength associated with the $|g\rangle$ to $|\nu\rangle$ electronic transition. Similarly, the TPA spectrum is related to the imaginary part of the third-order polarizability $\gamma(-\omega;\omega,\omega,-\omega)$ by

$$\delta(\omega) = \frac{4\pi^2\hbar\omega^2}{n^2c^2}L^4\text{Im}\langle\gamma\rangle \qquad (4)$$

where $\hbar$ is Plank's constant, c is the speed of light, n is the refractive index of the medium, L is the local field factor, and

$$\langle\gamma\rangle = \frac{1}{15}\left(3\sum_i \gamma_{iiii} + \sum_{j\neq i}(\gamma_{iijj} + \gamma_{ijij} + \gamma_{ijji})\right) \qquad (5)$$

is the orientational average of γ following eq 6 in ref 53. $\gamma(-\omega;\omega,\omega,-\omega)$ can been calculated as described in refs 32 and 46 and implemented in ref 47.

The calculated and experimental absorption maxima and transition dipole moments are compared in Table 1. As expected, the TDDFT reproduces the linear absorption spectra accurately, in particular the red-shift of the absorption maximum of **3R$_D$** and **5R**, compared to **3R**. However, the absorption of **7R$_D$** is red-shifted by ~0.2 eV in the TDDFT calculations, compared to the experiment. This shift can be ascribed to two reasons: (i) possible solute–solvent interactions, leading to geometrical distortions and limiting of the effective conjugation length to five repeat units (we estimate that torsional displacement of neighboring phenylenevinylenes by ~20° would be sufficient to reduce the saturation conjugation length) and (ii) an over-estimate of the exciton delocalization with the TDDFT approach, which, for example, gives ~10 repeat units for the exciton size in PPV compared to ~6–7 units observed in experiments.[44] Another feature that can be observed in both experimental and theoretical linear absorption spectra of the dimers is the strong Davydov splitting of the lowest electronic transition, due to the electrostatic interaction between the monomer transition dipoles and to the strong electronic exchange through the paracyclophane core upon dimerization (**3R** vs **3R$_D$**, **5R** vs **5R$_D$**, and **7R** vs **7R$_D$**). In particular, this electronic delocalization leads to an overall red-shift of the absorption band and to the appearance of both Davydov components in the linear absorption spectrum,[37] which makes these dimers different from the typical J (or H) aggregates.[54] We observe a shift of the center of the Davydov components compared to the monomer maximum of 0.05 and 0.03 eV in the spectra of **3R$_D$**, and **5R$_D$**, respectively, which is a consequence of overlap interactions. We further calculate splittings of 0.24, 0.17, and 0.12 eV in the spectra of **3R$_D$**, **5R$_D$**, and **7R$_D$**, respectively, which we attribute mostly to the dipolar interactions. The splitting decreases in the large dimers, since these have a reduced density of the excitonic wave function at the paracyclophane contact point and, therefore, have

a smaller interchromophore interaction. This trend is clearly seen in the experimental spectra as well (Figures 1 and 2).

The experimental and calculated transition dipole moments M_{ge} (contributions from both Davydov components have been included for the dimers) are in reasonably good agreement. However, the calculated transition dipoles systematically over-estimate the experimental ones. These quantities increase as the square root of the total number of double bonds in the molecule, which in turn indicates that the contributions to the oscillator strength ($f \sim M_{ge}^2$) from each repeat unit of the molecule are additive, a well-established trend in conjugated oligomers at the long-chain limit.[44]

Table 2 and Figure 3 show the theoretical and experimental TPA parameters and spectra, respectively. The two-photon cross sections obtained from theoretical calculations cannot be compared directly with the experimentally determined values, because the experimental spectrum has a finite width, due to broadening. To compare the experimental and theoretical data, it is common practice to introduce a line shape and bandwidth into the theoretical spectrum.[14,15,47,55,56] Various authors have used a bandwidth value of 0.1 eV for bands of Lorentzian shapes. Even though the choice of this specific value is somewhat arbitrary, a bandwidth of this order is comparable to the one observed experimentally for the chromophores for which it was originally used.[15] Since, in the cases under investigation here, the experimental bandwidths vary from band to band and from molecule to molecule (see Figure 3), we decided not to use a fixed line width in all cases. Instead the two-photon spectra were calculated from the theoretical cross sections derived from eq 4 by imposing Lorentzian band shapes and using linewidths (full width at half-maximum) given by $\Gamma = 2(\ln 2)^{0.5}\sigma$, where σ's are the parameters obtained from the fitting of the experimental spectra, as described above.

Additionally, in eq 4 we used the solvent parameters for toluene ($n = 1.494$) and the local field factor as calculated in the spherical cavity approximation, $L = (n^2 + 2)/3$, even though the calculations were performed on isolated molecules in the vacuum. At present, the effect of solvents on the two-photon properties of chromophores is not well understood. The study of the effect of the environment on the two-photon spectra of organic molecules is currently under investigation.

Overall, the TDDFT provides reasonably good agreement with the experiment with regard to both the energetics and the two-photon cross sections. The significance of this agreement must be tempered by the fact that there is uncertainty in the treatment of solvent effects and in the band shape. For example, an error of 10% in L would introduce an error of about 50% on δ. Nonetheless, the focus here is on the trends of the cross section and spectra, and conclusions on these aspects are not significantly affected by such uncertainties. We further note that the TPA peaks of **7R$_D$** are shifted to the red by 0.1 eV (peak *i*) and by 0.2 eV (peak *ii*) in the TDDFT calculations compared to the experimental results. This is similar to what is observed in the linear absorption spectrum and may be caused by the failure of the TDDFT to describe charge-transfer excitations, since higher lying A_g-type states in conjugated polymers correspond to excitations with well-separated electrons and holes.

Molecule **3R** and other structures closely related to it have been studied extensively in recent years, and it could be useful

(53) Garito, A. F.; Heflin, J. R.; Wong, K. Y.; Zamani-Khamiri, O. In *Organic Materials for Nonlinear Optics*; Hann, R. A., Bloor, D., Eds.; Royal Chemical Society, Burlington House: London, 1989; p 16.
(54) Silinsh, E. A.; Capek, V. *Organic Molecular Crystals*; AIP Press: New York, 1994.

to compare the theoretical results reported here with those obtained by different approaches. Albota et al.[14] used semiempirical INDO-MRD-CI calculations and obtained $\lambda^{(2)} = 595$ nm, $\delta = 680$ GM, and transition moments $M_{ge} = 13.3$ D and $M_{ee'} = 9.1$ D. Wang et al.[55] used the random phase approximation response theory at an ab initio level and obtained $\lambda^{(2)} = 542$ nm, $\delta = 636$ GM, $M_{ge} = 13.7$, $M_{ee'} = 3.1$. It can be seen that among these methods the TDDFT results ($\lambda^{(2)} = 715$ nm, $\delta = 824$ GM) give the closest agreement with the experiment for the energy of the two-photon state. The cross section from TDDFT is larger than those from the other two approaches mentioned above, but all can be considered to compare satisfactorily with the experimental value. The method reported by Das et al.,[56] based on a modified sum-over-state treatment at the semiempirical level, also yielded a good prediction of the energy of the two-photon state for this molecule ($\lambda^{(2)} = 708$ nm). However, the cross section calculated there was much smaller ($\delta = 180$ GM) than the experimental value, as was the estimate from another random-phase approximation calculation reported by Poulsen et al.[57] ($\delta = 120-170$ GM depending on the basis set). A comparison of the results of the TDDFT method with those from other theoretical methods and with experimental data for a wider series of chromophores was recently presented by Masunov et al..[47]

It is noteworthy that the TDDFT approach predicts that the TPA peaks are weakly affected by dimerization, whereas dimerization produces a strong Davydov splitting and red-shift in the linear absorption. The second Davydov component cannot be resolved in the experimental TPA spectra but appears as a shoulder on the low-energy side of peak *i* in the theoretical TPA spectra of the smallest dimer, **3R_D**. This component is not well-defined in the theoretical spectra of the larger dimers because of the congestion of electronic states in the high-frequency region. Calculations estimate the splittings in the TPA spectra of **3R_D**, **5R_D**, and **7R_D** to be 0.09, 0.07, and 0.05 eV, respectively. These energies are considerably smaller than those for the linear absorption case but follow the same trend as a function of chain length. These results indicate that intramolecular interactions through the **pCp** linkage strongly affect the B_u states but weakly perturb the A_g states because of the vanishingly small transition dipoles between A_g states. A detailed symmetry analysis of the point groups involved in the monomer and dimer transitions is given in the next section. However, the electron exchange interaction still leads to a weak splitting. This absence of strong interchromophore interactions for the two-photon absorption process in the dimer leads to a response that corresponds to additivity of the two monomeric units. In fact, calculations performed on a **5R_D** analogue, where the monomers were artificially separated by 20 Å to avoid through-space interaction, produced a TPA spectrum quite similar to that of **5R_D**. Strong electronic delocalization through the **pCp** core indeed leads to the appearance of new low-lying interchromophore electronic states, but these states do not contribute to the two-photon absorption. We further note that the density of electronic states in the two-photon region is increased in the dimers and in the **7R** monomer. Therefore, the

TPA intensity becomes "dispersed" among several nearly degenerate states.

Even though the TDDFT method does not calculate transition densities among excited states directly, it is possible to estimate these quantities using a perturbative expansion (eq 3.7 of ref 58). Subsequently, excited−excited-state transition dipole moments can be estimated. For comparison purposes, the calculated $M_{ee'}$ transition dipoles for the monomers are included in Table 3 (we did not compute these dipoles for the dimers because they have congested electronic spectra in the high-frequency region). Overall there is good agreement between experimental and calculated $M_{ee'}$ dipoles. However, in contrast with the linear absorption case, the calculations systematically underestimate the values of $M_{ee'}$.

We further observe the appearance of additional peaks in the TPA spectra computed with the TDDFT when going along the series **3R**−**5R**−**7R** and **3R_D**−**5R_D**−**7R_D**. These peaks indicate the presence of higher energy states that are two-photon allowed. These appear as small peaks on the blue side of the TPA spectra of **3R** (**3R_D**), increase in intensity for **5R** (**5R_D**) and become dominant in **7R** (**7R_D**) (see Figure 3). Calculations predict the appearance of a third TPA peak, *iii*, in the spectrum of the long monomers **5R** and **7R**. Due to the large computational effort involved, we were not able to calculate the high energy electronic states and, therefore, peak *iii* in the spectrum of the corresponding dimers **5R_D** and **7R_D**. The appearance of the high energy peaks *ii* and *iii* in the TPA spectra is related to the increase in the transition dipole moments from the band-gap $1B_u$ state to higher-lying A_g states with the increase in oligomer size.

Symmetry of Electronic States and Selection Rules for pCp Linked Dimers. The point group symmetry of the **3R**, **5R**, and **7R** monomer molecules is taken to be C_{2h}, which is the highest symmetry that would correspond to an idealized conformation of the conjugated backbone and neglect of the structure of the alkyl groups on the terminal amines. As is the case for simple polyenes in an ideal geometry, the π molecular orbitals of the **3R**, **5R**, and **7R** monomers transform as a_g and b_u in C_{2h}, as do the π electronic states of the molecules. For these oligomeric phenylenevinylene molecules, the lowest excited electronic state is of B_u symmetry and is one-photon active, whereas the lowest two-photon allowed state is of A_g symmetry and is forbidden in one-photon absorption.

When two monomer molecules of C_{2h} symmetry are connected through a **pCp** linkage as shown in Scheme 1, the dimer can be described as being of D_2 point group symmetry, which corresponds once again to the highest symmetry conformation and neglect of the alkyl group structure. The correlation of the symmetry species in C_{2h} and D_2 is as follows: A_g correlates to A and B_1 symmetry species and B_u correlates to B_2 and B_3 symmetry species.

The coupling of the π molecular orbitals of the monomers leads to splittings of the dimer π molecular orbitals into symmetric and antisymmetric combinations of the monomer orbitals of like symmetry. Considering the coupling of the lowest-energy a_g π molecular orbitals of the monomer, one obtains dimer π molecular orbitals which transform as a and b_1. The coupling of the b_u molecular orbitals of the monomers leads to b_2 and b_3 molecular orbitals for the dimer. Figure 5 displays a molecular orbital correlation diagram for the

(55) Wang, C.-K.; Macak, P.; Luo, Y.; Ågren, H. *J. Chem. Phys.* **2001**, *114*, 9813.
(56) Das, G. P.; Yeates, A. T.; Dudis, D. S. *Chem. Phys. Lett.* **2002**, *361*, 71.
(57) Poulsen, T. D.; Frederiksen, P. K.; Jørgensen, M.; Mikkelsen, K. V.; Ogilby, P. R. *J. Phys. Chem. A* **2001**, *105*, 11488.
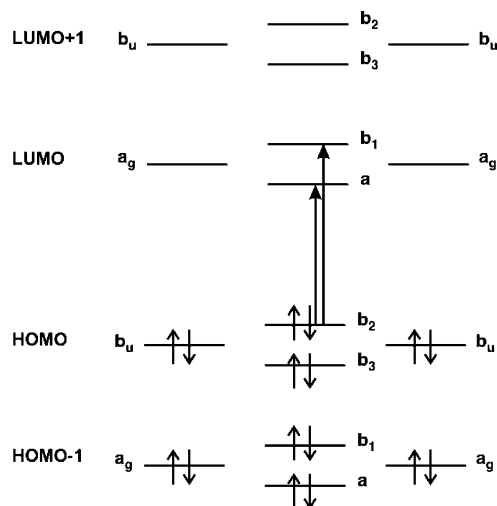
Figure 5. Correlation diagram for selected π molecular orbitals of the monomers and the **pCp** dimers. Two possible one-electron promotions that contribute to the lowest-energy B_2 and B_3 excited states of the dimer are illustrated.
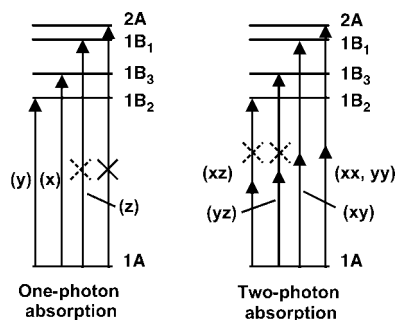

Figure 6. Qualitative energy level diagram and transitions for the **pCp** dimers showing the lowest five π electronic states. (Left) One-photon absorption transitions; polarizations are indicated in parentheses. The solid $\times$ indicates a symmetry forbidden transition, and the dotted $\times$ indicates a symmetry-allowed transition that is expected to be relatively weak. (Right) Two-photon absorption transitions; allowed tensor components are indicated in parentheses. The x direction corresponds to the long axis of the dimer molecule, and the z direction is perpendicular to the planes of the conjugated arms.

HOMO-1, HOMO, LUMO, and LUMO $+$ 1 π molecular orbitals of the monomers and the corresponding molecular orbitals of the **pCp** dimer. Considering the electronic configurations generated by single electron promotions, one finds that the symmetries of the π electronic states of the **pCp** dimer span the A, B_1, B_2, and B_3 representations (Figure 6; note that only a limited number of low-lying excited states is shown and that the ordering may vary).

The group theory analysis gives excited states of B_2 and B_3 symmetry that correspond to the splitting of the B_u excited states of the monomers and of B_1 and A symmetry corresponding to the A_g monomer excited states. The transitions from the ground state to both the B_2 and B_3 excited states are allowed in one-photon absorption, in contrast to dimer configurations that would preserve the center of symmetry. One of the dimer states, B_1, that correlates to an A_g state of the monomer is one-photon allowed, but the other, which is of A symmetry, is one-photon forbidden. The allowed component is z-polarized and is expected to be rather weak because of the limited amount of overlap and distance over which charge can be moved perpendicular to the molecular planes. All four possible two-photon transitions, i.e., $1A \rightarrow 1B_2$, $1A \rightarrow 1B_3$, $1A \rightarrow 1B_1$, and $1A \rightarrow 2A$, are symmetry

allowed. However, the transitions to $1B_2$ and $1B_3$ involve tensor components xz and yz, respectively, and are expected to be weak relative to the transitions to $1B_1$ (xy tensor component) and $2A$ (xx and yy tensor components) of which the latter should be the strongest transition.

Conclusion

In summary, we report the synthesis and characterization of a series of compounds that contains chromophores with large TPA cross sections held together via the **pCp** core. Within this structure the two TPA chromophores experience strong through-space delocalization. The key synthetic strategy involves sequential growth of an oligophenylenevinylene structure with dialkylamino and formyl substituents at the two termini of the conjugated framework and a Horner−Emmons coupling reaction with (4,7,12,15)tetra(diethylphosphonatemethyl)[2.2]paracyclophane. With the development of the modular synthesis scheme, examination of scaling conjugation length was also achieved. Significantly, the absorption spectra saturated with five repeat units. Theoretical calculations predict a further red-shifting with the seven-ring compound(s) but do not explicitly account for solvent dynamics.

Comparison of linear absorption and TPA reveals that the through-space delocalization influences one- and two-photon excitation processes differently. One observes a characteristic Davydov splitting of the monomer band into two components in the linear absorption spectra of their respective dimers. In contrast, distinct splitting is not observed in the case for the TPA spectra of dimers, where the contributions of the monomers to the cross sections are simply additive. Theoretical correlation of structure with optical information using TDDFT methods shows that this difference can be rationalized by noting that the linear and two-photon absorptions involve electronic states of different symmetry. Excited states of monomers with nearly B_u (odd) symmetry participate in the linear absorption, and near A_g (even) symmetry states participate in the TPA spectra. For the dimer states, which can be described as belonging to the D_2 point group, the strongest bands in the linear absorption spectra originate from transitions to B_2 and B_3 states. The two-photon spectrum, however, essentially contains transitions to A and B_1 states (the others being much weaker). The absorbed quantum of light induces changes of electronic density within each monomer (the diagonal elements of the transition density).[59] The electrostatic interaction between these induced charges leads to the splittings in the electronic spectra of dimers. For the dimer B_2 and B_3 states corresponding to B_u states of monomers, this interaction sums up leading to the large splittings observed in the linear spectra. In the case of dimer A and B_1 states correlating with A_g states, the cancellation of individual contributions results in the vanishingly small splittings in the ideal situation and leads to TPA spectra that are insensitive to the close proximity of the two chromophores. Study on a wider series of compounds would be necessary to assess whether the additivity in the two-photon cross section is characteristic of the chromophores studied here or is more general. In the recent literature, reports can be found of cases where the two-photon cross section increases linearly with the size of a dendrimer or

(58) Tretiak, S.; Chernyak, V.; Mukamel, S. *Int. J. Quantum Chem.* **1998**, *70*, 711.
(59) Tretiak, S.; Middleton, C.; Chernyak, V.; Mukamel, S. *J. Phys. Chem. B.* **2000**, *104*, 4519.

branched structure, as well as of cases where there is a superlinear increase. For example, Drobizhev et al.[27] found that the two-photon cross section increases almost linearly with the number of units in dendrimers based on 4,4′-bis(diphenylamino)-stilbene, even though they observed a significant increase going from the parent compound to the first generation dendrimer. Conversely, Chung et al.[24] reported that δ scales as 1:3.1:6.8 for chromophores containing, respectively, one, two, and three *N*-[4-{2-(4-{5-[4-(*tert*-butyl)phenyl]-1,3,4-oxadiazol-2-yl}phenyl)-1-ethenyl}phenyl]amine units. Similarly, δ increases more than linearly with the number of units in branched chromophores containing bis-1,4-(*p*-diphenylaminostyryl)-2,5-dicyanobenzene building blocks.[60] As a consequence, only a more extensive study will clarify the origin and details of the dependence of the two-photon properties on the type of building blocks, their connectivity, and the symmetry of the overall structure.

The fact that the spectral data are reasonably well reproduced by the theoretical calculations provides further support that the TDDFT method is a promising approach for the calculation of the TPA spectra of complex molecules, allowing an accurate prediction of the transition frequencies, of the number of two-photon allowed states in the visible and near-infrared excitation range, and of the evolution of the cross sections with molecular structure. Moreover it provides reasonable estimates for the actual cross sections. An appropriate description of dielectric environment and its effect on δ is currently a challenge for theoretical studies that warrants additional investigations.

The absence of a perturbation on the characteristics of TPA chromophores upon dimerization has implications from a materials perspective when one considers that many TPA applications benefit from, or rely upon, a high density of two-photon active chromophores. At high concentrations, or in the solid state, spectral positions and features of monomers in linear absorption can be superseded by absorption and emission characteristics of multichromophore systems in dimers and higher-order aggregates. Optical perturbations by aggregate formation tend to follow certain trends from the basic unit but are difficult to predict from the design of the monomer. Aggregate states are also often lower in energy and may dominate bulk behavior, regardless of their concentration. The results of this paper suggest that TPA properties can be less sensitive to aggregate perturbations. It should be possible to develop a more direct link between structure−property relationships of monomers and the performance in high concentration or in solid-state applications.

Experimental Details

Linear Absorption. All spectroscopic measurements were performed on toluene solutions (spectrophotometric grade, from Aldrich). UV−visible absorption spectra were recorded on a Shimadzu UV-2401 PC dual beam spectrometer or a Hewlett-Packard 8453 diode array spectrophotometer. Extinction coefficients, ϵ, were measured on multiple solutions obtained by dilution of two or three stock solutions. The measurements were performed using quartz cuvettes with path lengths of 0.1 and 1 cm. The solutions analyzed had concentrations between about 1×10^{-6} and 1×10^{-4} M. Fluorescence measurements were collected using a PTI fluorimeter at a detection angle of 90° relative to the excitation source. Quantum yields were determined

relative to 9,10-diphenylanthracene in degassed spectral grade cyclohexane.[61] The error associated with this technique is estimated to be ±5%.

Two-Photon Induced Fluorescence Measurements. The two-photon induced fluorescence method[40] was employed using both femtosecond and nanosecond pulsed lasers as excitation sources. Using a reference (*r*) chromophore for the two-photon cross section measurement, the δ for a sample (*s*) is given by:

$$\delta_s = \frac{S_s \Phi_{F(r)} \phi_r N_r}{S_r \Phi_{F(s)} \phi_s N_s} \delta_r \qquad (6)$$

where S is the detected two-photon induced fluorescence signal, Φ_F is the fluorescence quantum yield, and N is the concentration of the chromophore. ϕ is the collection efficiency of the experimental setup and accounts for the wavelength dependence of the detectors and optics as well as the difference in refractive indices between the solvents in which the reference and sample compounds are dissolved.[15] The measurements were conducted in a regime where the fluorescence signal showed a quadratic dependence on the intensity of the excitation beam, as expected for two-photon induced emission.

For the femtosecond-pulse experiment, the two-photon cross sections were measured using a Ti:Sapphire laser (Spectra-Physics, Tsunami) as the excitation source.[62] This laser generates ca. 85 fs pulses at a repetition rate of 82 MHz in the wavelength range 710−1000 nm. The reference standards used were fluorescein (in water, pH 11) and coumarin 307 (in methanol).[40] The concentrations of the solutions were in the range 5×10^{-6} to 2×10^{-5} M. The laser intensity at the sample was in the range 2×10^{8} to 2×10^{9} W/cm². The collection of the two-photon induced fluorescence signal was performed at the same detection wavelength for reference and sample compounds (530 nm). The output signal was averaged for 60 s for each excitation wavelength and sample. The nanosecond-pulse experiments were performed using an experimental setup in which the excitation source was a Nd:YAG pumped optical parametric oscillator (Quanta-Ray, MOPO 730) with a 5 ns pulse duration and 10 Hz repetition rate, tunable over the wavelength ranges 430−700 nm and 730−2000 nm.[15] The reference standards used in this case were fluorescein (in water, pH 11)[40] and *p*-bis(*o*-methylstyryl)benzene (in cyclohexane).[63] The concentrations of the solutions were in the range 7×10^{-5} to 1×10^{-4} M. The laser intensity was approximately $(1-5) \times 10^{7}$ W/cm² for the new compounds under investigation and up to 1×10^{8} W/cm² for the reference compounds. The data reported were averaged over 200 pulses at each wavelength. Please note that, for compounds **5R**, **5R_D**, and **7R_D**, the data collected below 685 nm are not reported here. The data points in this region were affected by relatively large fluctuations (large differences between independent measurements at the same wavelength). All the compounds studied were stable under the experimental conditions described here, and no bleaching of the solutions was observed at the end of the set of measurements.

General Synthetic Details. All synthetic manipulations were performed under an inert atmosphere in a nitrogen-filled glovebox or using Schlenk techniques. Tetrahydrofuran used for reactions was dried by stirring with Na metal overnight followed by degassing and vacuum transfer. All other reagents were obtained from Aldrich and were used as received. ¹H NMR spectra were obtained using a Varian Unity 400 MHz spectrometer. ¹³C NMR and 2D-¹H COSY spectra were obtained using a Varian Unity INOVA 500 MHz spectrometer. Mass spectrometry was performed by the UC Santa Barbara Mass Spectrometry Lab. HPLC was performed using a Shimadzu instrument equipped with a

(60) Yoo, J.; Yang, S. K.; Jeong, M.-Y.; Ahn, H. C.; Jeon, S.-J.; Cho, B. R. *Org. Lett.* **2003**, *5*, 645.

(61) Maciejewski, A.; Steer, R. P. *J. Photochem.* **1986**, *35*, 59.
(62) Wenseleers, W.; Stellaci, F.; Meyer-Friedrichsen, T.; Mangel, T.; Bauer, C. A.; Pond, S. J. K.; Marder, S. R.; Perry, J. W. *J. Phys. Chem. B* **2002**, *106*, 6853.
(63) (a) Fisher, W. G.; Wachter, E. A.; Lytle, F. E.; Armas, M.; Seaton, C. *Appl. Spectrosc.* **1998**, *52*, 536. (b) Kennedy, S. M.; Lytle, F. E. *Anal. Chem.* **1986**, *58*, 2643.

photodiode array detector. Reaction monitoring and separation were achieved with a nitro-derivatized silica HPLC column (ES Industries, catalog # 138213-NO2). The synthesis of **4**, **5**, **3R**, and **3R**$_D$ have been reported previously.[29]

4,4,5,5-Tetramethyl-2-(*para*-methyldiethylphosphonatephenyl)-1,3-dioxolane (1). Terephthaldehyde mono(diethylacetal) (10 g, 48 mmol) was diluted in ~35 mL of dry THF in a septum-covered 100 mL round-bottom flask charged with a Teflon-coated stir bar and maintained under an Ar atmosphere. The mixture was allowed to stir in a water bath at room temperature. Through the neck of the flask, 2 g (52 mmol) of NaBH$_4$ were added quickly to the mixture and the flask was resealed. The reaction was allowed to proceed for 3 h. Approximately 2 mL of water were added with stirring, and the THF was removed under vacuum. The resulting reaction crude was dissolved in CH$_2$Cl$_2$ and washed 3 times with deionized water, dried over MgSO$_4$, and filtered, and the solvent was removed under vacuum for a total of 10.0 g of the resultant benzyl alcohol (essentially quantitative yield). A portion (6.8 g, 32.3 mmol) of the product was dried in a round-bottom flask charged with a stir bar and fitted with a needle valve under vacuum on the Schlenk line overnight and then transferred to a glovebox. The material was dissolved in ~35 mL of dry benzene and stirred at rt. Then 3.5 g (13 mmol) of PBr$_3$ was added and allowed to react for 1 h. A brownish-white precipitate formed, and the reaction was quenched with water and diluted in CH$_2$Cl$_2$ and washed 4 times with brine. The resulting 4-formylbenzylbromide was completely deprotected (6.3 g, quantitative yield). The product was reprotected with pinacol in benzene with a trace of tosyl acid in a 250 mL round-bottom flask fitted with a Dean–Stark trap. The mixture was heated to 105 °C and allowed to react overnight. A small amount of powdered NaOH in dry ethanol was added to the cooled reaction mixture and allowed to stir for 30 min. This solution was filtered over Celite and washed 3 times with brine. GC/MS revealed complete protection. The solvent was dried and removed for a total of 9.6 g of product (94% yield). This material was transferred to a 100 mL round-bottom flask charged with a stir bar and fitted with a short path distillation head and receiving flask. Triethyl phosphite (8.0 g, 48 mmol) was added, and the reaction mixture was purged with argon and then heated to 130 °C overnight. The mixture was cooled, and the excess triethyl phosphite was removed by vacuum distillation. A total of 11.4 g (essentially quantitative yield) of **1** was collected. ^{1}H NMR (CDCl$_3$): 7.428 (d, 2H), 7.283 (dd, 2H), 5.951 (s, 1H), 3.981 (septet, 4H), 3.140 (d, 2H), 1.287 (d, 12 H), 1.240 (t, 6H). ^{13}C NMR (CDCl$_3$): 129.889, 236.717, 99.868, 82.844, 62.345, 34.404, 33.030, 24.496, 22.364, 16.568. EIMS: M$^+$ = 356.0.

4-Dihexylamino-4′-formylstilbene (2). A 250 mL round-bottom flask was charged with 3.47 g (12 mmol) of 4-dihexylaminobenzaldehyde, 5 g (14 mmol) of **1**, and a Teflon-coated stir bar and closed with a septum. Next, 60 mL of anhydrous DMF were transferred to the flask, and the mixture was stirred. The reaction mixture was cooled to 0 °C and 432 mg (18 mmol) of NaH was added through the neck of the flask. The reaction was allowed to warm to rt and react overnight. The crude product was diluted with CH$_2$Cl$_2$ and washed 3 times with brine. The organic layer was dried over MgSO$_4$ and filtered through a plug of silica over Celite to remove unreacted **1**. The solvent was removed under vacuum, and the resultant orange oil was diluted with ~150 mL of THF in a 500 mL flask. Approximately 350 mL of 10% HCl was added; the reaction flask was heated to 60 °C and stirred overnight. The THF was then removed under vacuum, and the remaining aqueous solution was extracted with CH$_2$Cl$_2$ and washed 3 times with deionized water. The organic layer was dried with MgSO$_4$ and filtered, and the solvent was removed under vacuum. An orange solid was collected and identified as **2** in 88% yield (4.13 g). ^{1}H NMR (CDCl$_3$): 9.962 (s, 1H), 7.831 (d, 2H), 7.596 (d, 2H), 7.418 (d, 2H), 7.204 (d, 1H), 6.906 (d, 1H), 6.634 (d, 2H), 3.304 (t, 4H), 1.608 (t, 4H), 1.339 (m, 12H), 0.930 (t, 6H). ^{13}C NMR (CDCl$_3$): 191.833. 148.643, 144.971, 134.516, 132.847, 130.473, 128.622, 126.338,

123.698, 122.097, 111.704, 51.261, 31.930, 30.519, 27.469, 22.910, 14.276. EIMS: M$^+$ = 391.6.

4-Dihexylamino-4′-formyldistyrylbenzene (3). A 100 mL round-bottom flask was charged with 1.83 g (4.7 mmol) of **2**, 2 g (5.6 mmol) of **1**, and a Teflon-coated stir bar and closed with a septum. Anhydrous DMF (~25 mL) was transferred to the flask, and the mixture was stirred. The mixture was cooled to 0 °C, and 168 mg (7 mmol) of NaH was added through the neck of the flask. The reaction was allowed to warm to rt and proceed overnight. Workup and the subsequent deprotection steps were similar to those used for **2** described in detail above. Additionally, a flash column (90 g silica, 60% CH$_2$Cl$_2$/40% hexanes) was necessary to isolate the desired compound. The product was collected as a red solid in 79% yield (1.83 g). ^{1}H NMR (CDCl$_3$): 9.998 (s, 1H), 7.875 (d, 2H), 7.660 (d, 2H), 7.503 (dd, 4H), 7.394 (d, 2H), 7.262 (d, 1H), 7.133 (d, 1H), 7.088 (d, 1H), 6.886 (d, 1H), 6.630 (d, 2H), 3.294 (t, 4H), 1.594 (t, 4H), 1.334 (m, 12H), 0.927 (t, 6H). ^{13}C NMR (CDCl$_3$): 191.833, 148.150, 143.901, 139.015, 135.313, 134.835, 132.263, 130.465, 129.752, 128.121, 127.446, 126.983, 126.490, 124.403, 123.053, 111.764, 51.276, 31.946, 30.519, 27.045, 22.910, 14.276. EIMS: M$^+$ = 493.7.

Bis(1,4)-(4″-(4′-dihexylaminostyryl)styryl)benzene (5R). A 25 mL round-bottom flask was charged with 274 mg (0.7 mmol) of **2**, 89 mg (0.234 mmol) of **5**, and a Teflon-coated stir bar and sealed with a septum. After the flask was flushed with argon, ~10 mL of dry THF was transferred to the flask and the mixture was stirred until dissolved. The flask was cooled to 0 °C, and 78 mg (0.7 mmol) of potassium *tert*-butoxide, dissolved in ~5 mL of dry THF, was transferred to the reaction mixture. The flask was allowed to warm to rt, and the reaction, to proceed overnight. The mixture was diluted in CH$_2$Cl$_2$ and washed 3 times with brine. The organic layer was dried over MgSO$_4$ and filtered, and the solvent was removed under vacuum. The crude was coated onto silica and was separated on a 90 g flash column with 20% CH$_2$Cl$_2$/hexanes as eluent, resulting in 152 mg (76% yield) of a bright yellow crystalline solid identified as the product. ^{1}H NMR (CDCl$_3$): 7.520 (s, 4H), 7.484 (d, 8H), 7.395 (d, 4H), 7.120 (d, 4H), 7.055 (d, 2H), 6.930 (d, 2H), 6.356 (d, 4H), 3.330 (t, 8H), 1.594 (t, 8H), 1.334 (m, 24H), 0.916 (t, 12H). EIMS: M$^+$ = 853.5

Tetra(4,7,12,15)-(4″-(4′-dihexylaminostyryl)styryl)[2.2]para-cyclophane (5R$_D$**).** A 25 mL round-bottom flask was charged with 712 mg (1.82 mmol) of **2**, 226 mg (0.3 mmol) of **4**, and a Teflon-coated stir bar and sealed with a septum. The mixture was flushed with argon, and ~10 mL of anhydrous DMF were transferred to the flask. The solids were dissolved, and the reaction mixture was cooled to 0 °C. A solution of 251 mg (2.2 mmol) of potassium *tert*-butoxide in ~2 mL of DMF was transferred to the flask, and the reaction mixture was allowed to warm to rt and react overnight. The mixture was diluted with CH$_2$Cl$_2$ and washed with deionized water and brine. The organic layer was dried over MgSO$_4$ and filtered, and the solvent was removed under vacuum, resulting in a bright orange solid. The solid was triturated in diethyl ether overnight and filtered off. The recovered solid was analyzed by HPLC with a nitro-derivatized silica column and found to contain only cis–trans isomers. The product was taken up in 500 mL of benzene, the solution was degassed, and the mixture was stirred overnight while being irradiated with a Hg lamp. The solvent was stripped, and HPLC analysis revealed a single peak. A total of 302 mg of bright orange solid was collected for a 60% yield. ^{1}H NMR (CDCl$_3$): 7.506 (dd, 16H), 7.450 (d, 8H), 7.298 (d, 4H), 7.133 (d, 4H), 7.045 (s, 4H), 6.975 (d, 4H), 6.957 (d, 4H), 6.663 (d, 8H), 3.364 (m, 4H), 3.316 (t, 16H), 2.930 (m, 4H), 1.627 (t, 16H), 1.356 (m, 48H), 0.936 (t, 24H). ^{13}C NMR (CDCl$_3$): 148.051, 138.052, 136.921, 136.193, 129.107, 128.591, 128.083, 127.173, 126.513, 124.722, 123.493, 111.832, 51.314, 33.410, 31.976, 27.523, 27.083, 22.940, 14.307. MS-MALDI/TOF: M$^+$ = 1756.0

Tetra(4,7,12,15)-(4‴-(4″-(4′-dihexylaminostyryl)styryl)styryl)[2.2]-paracyclophane (7R$_D$**).** A 25 mL round-bottom flask was charged with 444 mg (0.9 mmol) of **3**, 150 mg (0.2 mmol) of **4**, and a Teflon-coated

stir bar and sealed with a septum. The mixture was flushed with argon, and ~10 mL of anhydrous DMF were transferred to the flask. The solids were dissolved, and the reaction mixture was cooled to 0 °C. A solution of 112 mg (1 mmol) of potassium *tert*-butoxide in ~2 mL of DMF was transferred to the flask, and the reaction mixture was allowed to warm to rt and react overnight. The mixture was diluted with CH_2Cl_2 and washed with deionized water and brine. The organic layer was dried over $MgSO_4$ and filtered, and the solvent was removed under vacuum, resulting in a red oil. The recovered oil was separated by HPLC with a nitro-derivatized silica column (30% $CHCl_3$/Hexanes, 20 mL min^{-1}) and found to contain only cis−trans isomers. The product was taken up in 500 mL of benzene, the solution was degassed, and the mixture was stirred overnight while being irradiated with a Hg lamp. The solvent was stripped, and HPLC analysis revealed a single peak.

A total of 280 mg of dark red solid was collected for a 72% yield. ^{1}H NMR ($CDCl_3$): 7.511 (bm, 32H), 7.410 (d, 8H), 7.200 (m, 12H), 7.070 (m, 8H), 6.928 (m, 8H), 6.640 (d, 8H), 3.650 (m, 4H), 3.316 (t, 16H), 2.930 (m, 4H), 1.627 (t, 16H), 1.340 (m, 48H), 0.922 (t, 24H). MS-MALDI/TOF: M^+ = 2165.1.

JA038743I